Pergamon

Cement and Concrete Research 30 (2000) 709–713

CEMENT AND CONCRETE RESEARCH

Microstrain distribution in calcium hydroxide present in the interfacial transition zone

V.S. Harutyunyan[a], E.S. Abovyan[a], P.J.M. Monteiro[b,*], V.P. Mkrtchyan[a], M.K. Balyan[a]

[a]*Department of Solid State Physics, Yerevan State University, A. Manukyan 1, 375049 Yerevan, Armenia*
[b]*Department of Civil and Environmental Engineering, 725 David Hall, University of California at Berkeley, Berkeley, CA 94720, USA*

Received 12 February 1999; accepted 28 January 2000

Abstract

This article develops an approach for estimating the microstrain distribution along the thickness of the interfacial transition zone (ITZ) formed between aggregate and cement paste. This approach is dependent on the effectiveness of the X-ray's penetration depth into the sample and on the order of active reflection from calcium hydroxide (CH) texture. The ITZ was simulated by first casting cement paste on top of a polished flat substrate of granite. Next, the composite specimen was cured under saturated conditions and then broken at the substrate–cement paste interface for X-ray diffraction examination. Four orders (001, 002, 003, and 004) of reflection CoK_{α} from the CH texture were recorded. The experimental results indicate that the sizes and the microstrain of the CH crystallites decrease with increasing distance from the aggregate–cement paste interface.

Keywords: Elastic moduli; $Ca(OH)_2$; Modeling; X-ray diffraction

1. Introduction

The interfacial transition zone (ITZ) of concrete, a thin layer between the aggregate particle and the hydrate cement paste (HCP), is caused by the "wall effect," which prevents adequate packing of the cement grains close to the aggregate surface. The thickness of the ITZ ranges from 15 to 50 μm and depends on the fineness of the cement grains and the mineralogy of the aggregate. One of the principal differences between the HCP and the ITZ is a higher porosity in the ITZ [1,2]. The other essential structural distinction of the ITZ in comparison to HCP is the textured state of calcium hydroxide (CH) crystallites close to the aggregate surface [3,4]. The higher porosity and, in part, the textured state of the CH crystallites favor the appearance and development of the microcracks in the ITZ. These distinctions in the macrostructural states of HCP and the ITZ account for the lower microhardness [5], strength, and elastic moduli of the ITZ [1]. Nilsen and Monteiro [6] have shown that the ITZ has an effect on the overall elastic moduli of concrete.

Although the porosity profiles in the ITZ of concrete have been measured [7,8], no direct measurements of elastic moduli profiles within this transition zone are yet available. By comparing model predictions to measured data of the overall elastic moduli of concrete, however, the elastic moduli profiles [9] and their effective values [10] within the ITZ have been obtained. The research described below investigated the elastic properties of the ITZ on a micromechanical/microstructural level by conducting X-ray diffraction measurements of strain distribution within the ITZ. X-ray diffraction peaks from crystalline components of the ITZ of concrete—in particular from CH—was recorded, with the goal of developing truly realistic models.

Recent research of X-ray diffraction measurements of strain in CH texture of the ITZ have been carried out [11,12]. Because only about 25% of the volume of the ITZ in cement paste contains CH crystallites, measurement of microstrain in CH texture cannot characterize the entire strain field in the ITZ, whose components have different elastic properties. However, information on the microstrain distribution in CH texture may provide insight on the strain gradient within the ITZ.

The aim of this research is to develop an approach for estimating microstrain distribution along the thickness of the ITZ of concrete. This approach is dependent on the

* Corresponding author. Tel.: +1-510-643-8251; fax: +1-510-643-8928.
E-mail address: monteiro@ce.berkeley.edu (P.J.M. Monteiro).

0008-8846/00/$ – see front matter
PII: S0008-8846(00)00230-1

effectiveness of X-ray's (i.e., maximum) penetration depth into the sample and on the order of active reflection from CH texture.

2. Theoretical approach

Before deriving an expression for the effective penetration depth of X-ray into the specimen of HCP, let us review the following well-known factors:

(1) The ITZ contains CH crystallites [1].

(2) A CH crystallite is composed of a hexagonal crystallographic structure [2], with the crystallographic *c*-axis parallel to its unit vector $\boldsymbol{n}$ of physical surface (see Fig. 1). Therefore, the system of the atomic planes (0001) of crystallite is parallel to its physical surface (i.e., to entrance surface for the X-rays).

(3) In the ITZ, the CH crystallites are configured in an axially textured state [3]. The axis of their texturation is parallel to the normal $\boldsymbol{n}_s$ to the external interface of the ITZ (i.e., is parallel to the *z*-axis, see Fig. 1).

Let us assume that the HCP is separated from the aggregate and that it contains the ITZ (see Fig. 1; the top layer of specimen is the ITZ). Note in Fig. 1 the rectangular coordinate system *x*,*z*. The *z*-axis is perpendicular to the external plane interface of the ITZ.

The absorption of X-ray radiation propagating in non-homogeneous polycrystalline material can be taken into account by the Eq. (1):

$$I = I_0 \exp\left[-\int_s \mu(s)\mathrm{d}s\right] \tag{1}$$

where I_0 is the intensity of the incident X-ray beam, (*s*) is the ray path, $\mu(s)$ is the linear normal absorption coefficient of X-rays at each point on the ray path, and *I* is the intensity of the X-ray beam after it has traversed path (*s*) and the line integral is taken along path (*s*).

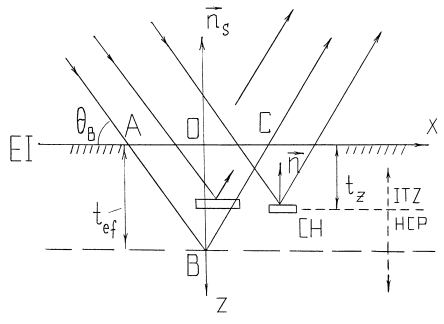

Fig. 1. The scheme of X-ray diffraction on CH texture of the ITZ of concrete. The ITZ is the interfacial transition zone of concrete, HCP is the hydrated cement paste of concrete, EI is the external interface of the ITZ, t_z and t_{ef} are the thickness and the effective depth of X-ray penetration, respectively.

Because of a considerable gradient of porosity, the ITZ of concrete is non-homogeneous (the gradient of porosity is directed towards the negative direction of the *z*-axis, see Fig. 1). The effective linear absorption coefficient, μ_{ef}, of the ITZ can be defined as follows:

$$I = I_0 \exp\left[-\int_s \mu(s)\mathrm{d}s\right] = I_0 \exp[-\mu_{ef} L_s] \tag{2}$$

where

$$L_s = \int_s \mathrm{d}s \tag{3}$$

L_s is the length of X-ray path in the ITZ. Within the ITZ, there is a gradient of material density [2], therefore, the real path of X-rays in HCP, both in transmission and reflection (from CH texture) directions, should be curved. This leads to a variation of the refraction index from point-to-point (the gradients of material density and refraction index are directed towards the positive direction of the *z*-axis).

Because the refraction index for X-rays is close to unity and depends slightly on the non-uniformity of a material, our investigation assumed that the path of X-rays, both in transmission and reflection directions, might be approximated by a straight section. Therefore, using Eq. (3), the effective penetration depth, t_{ef}, of X-rays becomes

$$L_s = AB + BC = 2t_{ef}/\sin\theta_{Bh} \tag{4}$$

where *AB*+*BC* is the total length of the path (*s*) of X-rays with the maximal penetration into the HCP, θ_{Bh} is the exact Bragg's angle of X-ray diffraction on CH crystallites of the ITZ, and index *h* indicates the order of the reflection. After substituting Eq. (4) into Eq. (2), Eq. (2) becomes:

$$I = I_0 \exp[-2\mu_{ef} t_{ef}/\sin\theta_{Bh}] \tag{5}$$

where the value μ_{ef} is the effective absorption coefficient of the ITZ. By defining the value t_{ef} from Eq. (5) through the condition:

$$I/I_0 = \exp[-2\mu_{ef} t_{ef}/\sin\theta_{Bh}] = 0.1 \tag{6}$$

i.e., in accordance with the requirement that the intensity of X-rays on their "longest way," L_s, given by Eq. (4), decreases by an order. The following expression [Eq. (7)] for t_{ef} is obtained from Eq. (6):

$$t_{ef} \approx \sin\theta_{Bh}/\mu_{ef.} \tag{7}$$

For X-ray 00*h* reflection from CH texture, Bragg's law is expressed as:

$$2d_h \sin\theta_{Bh} = \lambda \tag{8}$$

where λ is the wavelength of X-ray radiation, and d_h is the interplanar spacing of (00*h*) reflecting atomic planes. For CH crystallites, which have a hexagonal crystallographic structure,

$$d_h = c/h \tag{9}$$

where c is the lattice spacing along the crystallographic c-axis (for CH crystallite c = 0.4909 nm). The linear absorption coefficient for monochromatic X-ray radiation is given by the expression [13]:

$$\mu_{ef} = k\lambda^3 \tag{10}$$

where k is the coefficient dependent on the chemical composition of the material and its density. Taking into account Eqs. (8)–(10), Eq. (7) becomes

$$t_{ef} = h/2kc\lambda^2 \tag{11}$$

Eq. (11) demonstrates that the effective depth of radiation penetration into the polycrystalline material essentially depends on the radiation wavelength and on the order of reflection.

Harutyunyan [14] has developed the following expression for the integral width, β_i, of X-ray diffraction peaks detected from polycrystalline structure (or weakly expressed texture), provided that the incident radiation is monochromatic and the instrumental aberrations equal to zero:

$$\begin{aligned}\beta_i^2(h) &= [8\pi\tan^2\theta_{Bh}\langle\varepsilon^2\rangle + (\lambda/\cos\theta_{Bh}l_m)^2] \\ &\quad \times [1 - a\sigma_l^2(2d_h^{-2}\langle\varepsilon^2\rangle + \pi^{-1}l_m^{-2})] \\ &\equiv F_h(l_m, \sigma_l, \langle\varepsilon^2\rangle)\end{aligned} \tag{12}$$

where $\langle\varepsilon^2\rangle$ is the square of the mean-square strain of crystallites, l_m and σ_l are the prevalent value and the standard deviation of crystallite thickness along the crystallographic c-axis, respectively; and a is the constant coefficient.

If we do not take into account the dispersion of particles thickness in our analysis of the experimental results, after the substitution $\sigma_l = 0$ into Eq. (12), we obtain:

$$\beta_i^2(h) = [8\pi\tan^2\theta_{Bh}\langle\varepsilon^2\rangle + (\lambda/\cos\theta_{Bh}l)^2 \equiv F_h(1, \langle\varepsilon^2\rangle) \tag{13}$$

where l represents the crystallites' mean thickness. It follows from Eq. (13) that by solving the set of two simultaneous equations

$$\left\{\beta_i^2(h) = F_h(l, \langle\varepsilon^2\rangle)\right\} \text{ for } h = p, q \tag{14}$$

the value l and the mean-square strain $(\langle\varepsilon^2\rangle)^{1/2}$ can be found. Eq. (14) assumes that $h = p,q$ are two possible different orders of the same reflection h. From Eqs. (11) and (13), it is clear that the connection between the values t_{ef} and $(\langle\varepsilon^2\rangle)^{1/2}$ can be stated through the order of reflection h (see Table 2).

3. Experimental procedure

The composite specimen was prepared by casting Portland cement paste with a water–cement ratio of 0.35 on top of a polished flat substrate of granite. Next, the specimen was cured under saturated conditions for 5 years and then broken at the substrate–cement paste interface for X-ray diffraction examination (see Fig. 1). X-ray diffraction investigations of the sample were carried out using the Bragg–Brentano focusing scheme and θ–2θ mode of detection of diffracted radiation. Four orders (001, 002, 003, and 004) of reflection 001 CoK_α from the CH texture were recorded. For monochromatization of the radiation, a graphite monochromator was used. The width of both incidence and receiving slits was of the order of 0.1 mm. The diffraction pattern contained pairs of partially overlapping peaks, which corresponded to both the $K_{\alpha1}$ and $K_{\alpha2}$ lines. The procedure of diffraction peaks treatment (the separation and the profile fitting of overlapping peaks) is described in detail by Abovyan et al. [11] and Harutyunyan et al. [12]. By direct measurements of the linear absorption coefficient of HCP, the value $\mu_{ef} \approx 15$ cm^{-1} were obtained for MoK_α radiation.

4. Analysis of experimental results

Using the measurement value of absorption coefficient, $\mu_{ef} \approx 15$ cm^{-1}, obtained for MoK_α radiation, the corresponding values μ_{ef} and t_{ef} were estimated for different wavelengths of X-ray characteristic radiation and four orders of the reflection 001 in compliance with Eqs. (10) and (11). The relevant values of this estimation are presented in Table 1.

Solving the two simultaneous equations in Eq. (14) (the equations are given by Eq. (13), into the left-hand side of which the integral width, β_i, of the relevant 00h $K_{\alpha1}$ line is substituted) for three pairs {001, 002}, {002, 003}, {003, 004} of reflections {00h} (h = 1; 2; 3; 4), the values of the average thickness, l, and the mean-square strain, $(\langle\varepsilon^2\rangle)^{1/2}$, of CH crystallites in the ITZ and partially in bulk HCP were obtained for the wavelength of $CoK_{\alpha1}$ radiation. The relevant data are listed in Table 2.

In Table 2, the values l = 0.26 μm and $(\langle\varepsilon^2\rangle)^{1/2} = 3.7 \times 10^{-4}$ (obtained using reflections 001 and 002) are the

Table 1
The values of the linear absorption coefficient and the effective depth of penetration for HCP (water–cement ratio = 0.35) obtained for different wavelengths of X-ray radiation

Radiation	Absorption coefficient, μ_{ef} (cm^{-1})	Effective depth of penetration, t_{ef} (μm)			
		Reflection 001	Reflection 002	Reflection 003	Reflection 004
MoK_α	15	122	244	366	488
CuK_α	120	26	52	78	104
CoK_α	251	19	38	57	76
CrK_α	525	12	24	36	48

Table 2
The values of the average thickness, l, and the mean-square strain, $(\langle\varepsilon^2\rangle)^{1/2}$, of CH crystallites in the ITZ and partially in bulk HCP obtained with CoK_α radiation

Pair of reflection	Order of reflection, h	t_{ef} (μm)	l (μm)	$(\langle\varepsilon^2\rangle)^{1/2}$
001	1	19		
002	2	38	0.26	3.7×10^{-4}
002	2	38		
003	3	57	0.24	3.4×10^{-4}
003	3	57		
004	4	76	0.20	2.9×10^{-4}

average structural characteristics of CH texture within the region $0 \le z \le t_{ef}$ ($h = 2$) = 38 μm. The upper limit of this region is the penetration depth of radiation for reflection 002, whereas the lower limit is defined by the origin of the coordinate system xOz (see Fig. 1). In an analogous way, the data $\{l = 0.24$ μm, $(\langle\varepsilon^2\rangle)^{1/2} = 3.4 \times 10^{-4}\}$ and $\{l = 0.20$ μm, $(\langle\varepsilon^2\rangle)^{1/2} = 2.9 \times 10^{-4}\}$ are the average characteristics of the CH texture in the ITZ within the regions $0 \le z \le t_{ef}$ ($h = 3$) = 57 μm and $0 \le z \le t_{ef}$ ($h = 4$) = 76 μm, respectively. Clearly, there will be a certain degree of overlap between the "X-ray information" coming from successive layers of the object. Therefore, the data of the value $(\langle\varepsilon^2\rangle)^{1/2}$ in Table 2 does not refer to the real exact strain profile $\varepsilon(z)$ within the object under investigation, but describes semi-quantitatively the spatial distribution of microstrain.

Because of the condition (see Table 2), [Eq. (15)]:

$$t_{ef}(h = 3) \approx t_z \approx 50\text{mm} \le t_{ef}(h = 4) \tag{15}$$

where t_z is the thickness of the ITZ (1,2), the data $\{l = 0.20$ μm, $(\langle\varepsilon^2\rangle)^{1/2} = 2.9 \times 10^{-4}\}$ in the third row of the Table 2 partially characterizes the structural state of CH crystallites in the thin layer of HCP within the 50 μm $\le z \le t_{ef}$ ($h = 4$) = 76 μm region.

Fig. 2 presents plots of the microstrain, $(\langle\varepsilon^2\rangle)^{1/2}$, and the average thickness, l, of the CH crystallites vs. depth of the ITZ and partially of bulk HCP, which schematically demonstrates the increase of effective penetration depth, t_{ef}, depending on the order of active reflection.

From the data presented in Table 2, it follows that the sizes of CH crystallites decrease from the external interface of the ITZ (towards the positive direction of the z-axis; see Fig. 1). This qualitatively correlates with the data presented by Mehta and Monteiro [1] and Maso [2]. Typically, images obtained from SEM studies show much bigger CH crystals [15]. This study, however, includes small CH crystals engulfed in the CSH and takes into account that large CH crystals may be formed by many smaller CH crystallites.

In order to fracture the composite specimen at the aggregate–cement paste interface, the specimen was exposed to low humidity. This generated drying shrinkage in the cement paste, which then detached from the substrate, suggesting that some part of CH crystallites in the ITZ has compressive microstrains (i.e., the crystal lattice in these crystallites is subjected to compressive strain along the crystallographic c-axis). We cannot exclude, however, the possibility that CH crystallites will be subjected to tensile microstrains or do not contain any strain because of creep in cement paste during its drying. To some degree, the data contained in Table 2 provides information on the gradient of microstrain distribution within the ITZ and partially within the HCP. Additional study should be conducted to determine the microstrain distribution in ettringite crystallites.

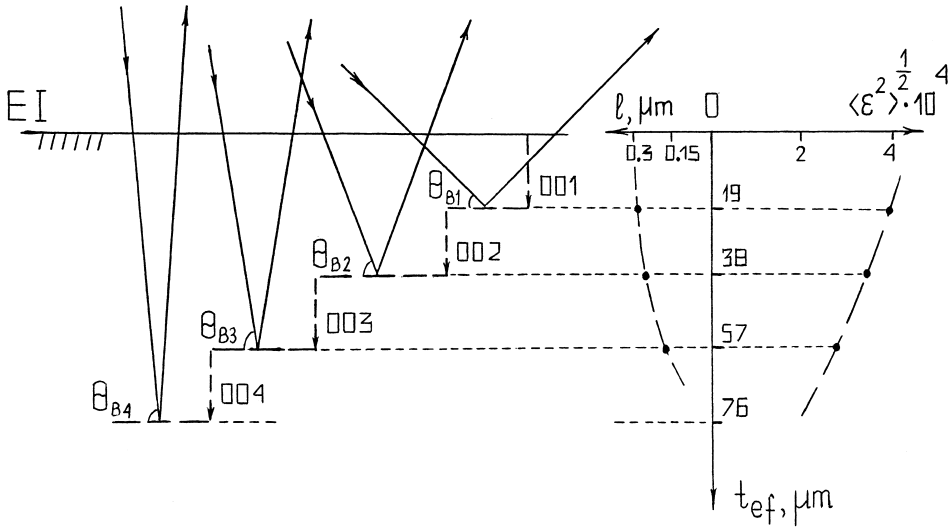

Fig. 2. The diagram (the left-hand side) represents the dependence of t_{ef} on the order of reflection. The plots (the right-hand side) of the values l and $(\langle\varepsilon^2\rangle)^{1/2}$ vs. the depth of the ITZ are shown.

5. Conclusions

A new method is proposed to estimate the microstrain and crystal size distribution of CH in the ITZ. A mathematical formation, based on the dependence of the X-ray's effective penetration depth into the sample and on the order of active reflection from CH texture, is developed.

Experimental studies were performed on a composite specimen of cement paste cast on top of a polished surface of granite. Reflections 001 and 002 of CH within the region of 38 μm in the ITZ indicate that the average size and microstrain is 0.26 μm and 3.7×10^{-4}, respectively. Using higher order reflections, the average size and microstrain is $\{0.24\ \mu m, 3.4 \times 10^{-4}\}$ and $\{0.20\ \mu m, 2.9 \times 10^{-4}\}$ within the $0 \leq z \leq 57$ μm and $0 \leq z \leq 76$ μm regions, respectively. These results confirm that the sizes and microstrain of the CH crystallites decrease with increasing distance from the aggregate–cement paste interface.

Acknowledgments

The authors would like to thank Dr. A.P. Aivazian and Prof. H.R. Wenk for valuable discussions. The research described here was made possible in part by Award No. AE1-103 of the U.S. Civilian Research and Development Foundation for the Independent States of the Former Soviet Union (CRDF).

References

[1] P.K. Mehta, P.J.M. Monteiro, Concrete: Structure, Properties and Materials, Prentice-Hall, New York, (1993) p. 38.
[2] J.C. Maso, Rilem Report 11: Interfacial Transition Zone in Concrete, E&FN SPON, Chapman & Hall, London, (1996).
[3] J. Grandet, J.P. Ollivier, 7e Congres International de la Chimie des Ciments, Vol. 3 (1980) VII-85–VII-89.
[4] R. Detwiler, P.J.M. Monteiro, H.R. Wenk, Z. Zhong, Texture of calcium hydroxide near the cement paste–aggregate interface, Cem Conc Res 18 (1988) 823–829.
[5] T.Y. Lyubimova, E.R. Pinus, Kolloidn Zh 24 (5) (1962) 578–587.
[6] A.U. Nilsen, P.J.M. Monteiro, Concrete: A three phase material, Cem Concr Res 23 (1993) 147–151.
[7] K.L. Scrivener, E.M. Gartner, Microstructural gradients in cement paste around aggregate particles, bonding in cementitious composites, in: S. Mindess, S.P. Shah (Eds.), Materials Research Society, Vol. 114, Pittsburgh, PA, (1989) 77–85.
[8] M.P. Lutz, R.W. Zimmerman, Effect of the interphase zone on the bulk modulus of a particulate composite, J Appl Mech 63 (1996) 855–861.
[9] M.P. Lutz, P.J.M. Monteiro, Microstructure of cement-based systems/bonding and interfaces in cementitious materials, Proc Material Research Society 370 (1995) 413–418.
[10] G. Ramesh, E.D. Sotelito, W.F. Chen, Effect of transition zone on the elastic moduli of concrete materials, Cem Concr Res 26 (1996) 611–622.
[11] E.S. Abovyan, P.J.M. Monteiro, V.S. Harutyunyan, V.P. Mkrtchyan, M.K. Balyan, J Appl Phys, submitted for publication.
[12] V.S. Harutyunyan, E.S. Abovyan, P.J.M. Monteiro, V.P. Mkrtchyan, M.K. Balyan, J Appl Cryst, submitted for publication.
[13] Ya.S. Umanskii, Yu.A. Skakov, A.N. Ivanov, L.N. Rastorguyev, Crystallography, Roentgenography and Electron Microscopy, Metalurgiya, Moscow (1982).
[14] V.S. Harutyunyan, J Mater Res, submitted for publication.
[15] P.J.M. Monteiro, J.C. Maso, J.P. Ollivier, The aggregate–mortar interface, Cem Concr Res 15 (1985) 953–958.